Suppression of Axial Methionine Fluxion in *Hydrogenobacter thermophilus* Gln64Asn Cytochrome c_{552}[†]

Xin Wen and Kara L. Bren*

Department of Chemistry, University of Rochester, Rochester, New York 14627-0216

Received November 20, 2004; Revised Manuscript Received February 2, 2005

ABSTRACT: Proteins in the cytochrome *c* (cyt *c*) family with His-Met heme axial ligation display diverse heme electronic structures as revealed by the NMR spectra of their oxidized (paramagnetic) forms. These variations in electronic structure are thought to result primarily from differences in heme axial Met orientation among cyt *c* species. The factors determining Met orientation in cyts *c*, however, remain poorly understood. An additional layer of complexity was revealed with the recent finding that the axial Met in *Hydrogenobacter thermophilus* cytochrome c_{552} (*Ht* cyt c_{552}) is fluxional, sampling two conformations rapidly on the NMR time scale, resulting in an unusual compressed range of heme substituent hyperfine shifts [Zhong, L., Wen, X., Rabinowitz, T. M., Russell, B. S., Karan, E. F., and Bren, K. L. (2004) *Proc. Natl. Acad. Sci. U.S.A. 101*, 8637−8642]. In this work, the ^{1}H NMR hyperfine shift pattern of *Ht* cyt c_{552} is drastically altered by making the conservative heme pocket mutation Gln64Asn. The mutant (*Ht* Q64N) displays a pattern of heme hyperfine shifts with a remarkable resemblance to that of structurally homologous *Pseudomonas aeruginosa* cyt c_{551}, which has Asn at position 64 and a single heme axial Met conformation. NMR analysis reveals that Asn64 in *Ht* Q64N is positioned to interact with the axial Met61, whereas the Gln64 in wild-type *Ht* cyt c_{552} is not. It also is found that the heme axial Met is not fluxional in *Ht* Q64N and has an orientation similar to that in *P. aeruginosa* cyt c_{551}. These results indicate that peripheral interactions with the axial Met play an important role in determining axial Met orientation and heme electronic structure in cyts *c*.

Nature presents a diverse range of coordination environments for metal ions within metalloproteins (*1*). In electron transfer proteins, it is generally thought that the protein maintains a metal coordination environment that does not change significantly in response to oxidation state. A fixed metal environment is important functionally for minimizing reorganization energy for electron transfer and for protecting the metal ion from the binding of solvent and other exogenous ligands (*2*). The control of the metal coordination sphere in an electron transfer protein comes from a combination of metal site burial and definition of the metal-binding site by the protein scaffold and/or any metal-binding cofactor. Coordination sites in small metal complexes, in contrast, often display ligand rearrangements. One type of rearrangement common in inorganic and organometallic chemistry is described as fluxion, which is the rapid rearrangement of metal−ligand bonding (*3*, *4*). Because of the constraints placed by the protein structure, fluxional behavior is not generally considered when evaluating conformations of amino acid ligands to metal sites within proteins. Recently, however, two cases of fluxionality of methionine ligands to heme iron in electron transfer proteins have been reported. This behavior has been observed in cytochromes c_{552} (cyts c_{552})[1] from *Hydrogenobacter thermophilus* (*Ht*) (*5*) and *Nitrosomonas europaea* (*Ne*) (*6*). The dynamic process is proposed to be inversion through the Met ligand thioether sulfur, occurring on the microsecond time scale at room temperature (*5*) (illustrated by the arrow in Figure 1A). Although it is possible that such ligand dynamics exist in other metalloproteins, it also is thought that in most cyts *c* the axial Met is not fluxional (*7*, *8*). This raises the question of the physicochemical basis for Met fluxion in *Ht* and *Ne* cyts c_{552}. Understanding the factors causing Met fluxion in these cyts *c* is important for understanding methionine−metal interactions in metalloproteins in general.

NMR spectroscopy is useful for characterizing both dynamics of proteins and fluxional behavior of inorganic complexes. The paramagnetism ($S = {}^1/_2$) of oxidized cyts *c* makes these proteins particularly attractive for NMR study of heme−ligand interactions and is the property that facilitated detection of the novel Met dynamics in *Ht* and *Ne* cyts c_{552} (*5*, *6*). Particularly useful are the resonances of the methyl groups in the α position relative to the heme macrocycle (at positions 1, 3, 5, and 8; Figure 1). The hyperfine shifts of the heme methyls are determined primarily by the Fermi contact shift, which results from unpaired electron spin density at the resonant nucleus (*9*−*12*). The contact shift, in

[†] This work was supported by National Institutes of Health Grant GM63170.

* To whom correspondence should be addressed. Telephone: (585) 275-4335. Fax: (585) 276-0205. E-mail: bren@chem.rochester.edu.

[1] Abbreviations: CD, circular dichroism; cyt *c*, cytochrome *c*; cyt c_{552}, cytochrome c_{552}; *Ht* cyt c_{552}, *Hydrogenobacter thermophilus* cytochrome c_{552}; *Ht* Q64N, *Hydrogenobacter thermophilus* Gln64 → Asn cytochrome c_{552}; *Ne* cyt c_{552}, *Nitrosomonas europaea* cytochrome c_{552}; NMR, nuclear magnetic resonance; NOE, nuclear Overhauser effect; *Pa* cyt c_{551}, *Pseudomonas aeruginosa* cytochrome c_{551}; *Sc* cyt *c*, *Saccharomyces cerevisiae* iso-1-cytochrome *c*.

10.1021/bi047556+ CCC: $30.25
Published on Web 03/09/2005

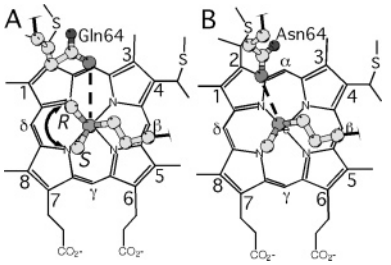

FIGURE 1: (A) Proposed orientations of side chains of Met61 and Gln64 in *Ht* cyt c_{552}. Shown are the Gln64 position from the NMR structure of reduced *Ht* cyt c_{552} [first structure of ensemble, PDB identifier 1AYG (*20*)] and the proposed conformations of the axial Met61 from analysis of oxidized *Ht* cyt c_{552} NMR (*5*). *R* and *S* indicate the conformations with the indicated chirality at the Met sulfur. (B) Orientations of Asn64 and Met61 in *Pa* cyt c_{551} from the X-ray crystal structure [351C (*22*)]. The plane of the axial His (not shown) lies approximately along the heme α−*γ-meso* axis in both proteins (*22*, *39*). The measured distance between the residue 64 side chain Nϵ and the axial Met Sδ (dashed line) is (A) 4.9−6.1 Å (range in family of NMR structures) and (B) 3.6 Å. The heme substituent numbering system used in the text is shown.

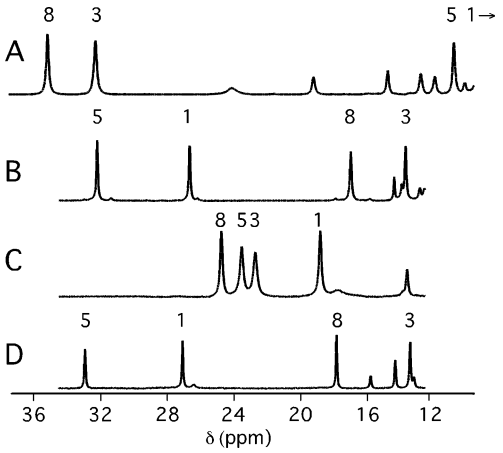

FIGURE 2: Downfield regions of 500 MHz ^{1}H NMR spectra of oxidized (A) horse heart cyt *c* (50 mM sodium phosphate, pH 7.0) (*46*), (B) *Pa* cyt c_{551} (50 mM sodium phosphate, pH 6.0) (*25*), (C) *Ht* cyt c_{552} (120 mM sodium acetate-d_3, pH 5.0) (*5*), and (D) *Ht* Q64N (120 mM sodium acetate-d_3, pH 5.0). Heme methyl assignments are indicated. See Table 1 for shifts of selected heme substituents.

turn, is determined primarily by the details of the heme−ligand interactions. The orientations of both heme axial ligands with respect to the in-plane heme axes determine the unpaired electron spin distribution on the heme macrocycle and, thus, the heme substituent contact shifts (*9*, *10*, *13*). In cyts *c*, the axial His is generally aligned along the α−*γ-meso* axis, but the axial Met is found in different conformations in different cyt *c* species (*7*, *8*). Cyts *c* with the axial Met oriented as in Figure 1A with the prochiral sulfur in the *R* configuration exhibit a pairwise ordering of heme methyl shifts with methyls 8 and 3 downfield of methyls 5 and 1 (shift ordering 8-CH_3 > 3-CH_3 > 5-CH_3 > 1-CH_3). An example is horse cyt *c* (Figure 2A). In contrast, cyts *c* with the axial Met in the *S* configuration (Figure 1) show a reversed pattern, with methyls 5 and 1 appearing downfield of methyls 8 and 3 (5-CH_3 > 1-CH_3 > 8-CH_3 > 3-CH_3) (*14*, *15*). The prototypical example of this type of cyt *c* is *Pseudomonas aeruginosa* (*Pa*) cyt c_{551} (Figure 2B). A large difference in heme substituent chemical shifts results from this difference in Met configuration because the ligand

FIGURE 3: Three-dimensional structure of *H. thermophilus* cyt c_{552} (PDB identifier 1AYG; first structure of ensemble) (*20*). Other members of the cyt c_8 structural family, having similar 3-D structures, include *P. aeruginosa* cyt c_{551} (*22*) and *N. europaea* cyt c_{552} (*21*).

configuration change corresponds to a reorientation of the Met ligand *p* orbital angle[2] relative to the iron *d* orbitals and the porphyrin 3e(π) orbitals, and these interactions ultimately determine unpaired electron spin distribution on the heme macrocycle (*10*, *13*, *14*).

The hypothesis that *Ne* and *Ht* cyts c_{552} display axial Met fluxion arose from the observation that all four heme methyl resonances in the NMR spectra of the ferric proteins have similar shifts (*5*, *6*, *16*, *17*). The proposed cause of the compressed heme methyl shift range is an averaging between the spectra corresponding to the *R* and *S* configurations (Figure 2) and is consistent with T_1-independent line broadening of the heme methyl ^{1}H resonances seen in both of these proteins (*5*, *6*). In *Ht* cyt c_{552}, it also was determined that the orientation of the magnetic axes, which is determined by the orientations of the heme axial ligands (*18*, *19*), is consistent with conformational averaging from Met fluxion (*5*). Although fluxionality of a heme axial Met within two proteins now has been characterized, the basis for the existence of this behavior in these cytochromes is not understood.

Ht cyt c_{552} (*20*) and *Ne* cyt c_{552} (*21*) are both members of the cyt c_8 structural subclass (Figure 3), which also claims the nonfluxional *Pa* cyt c_{551} as a member (*22*). The question is thus raised as to why in particular *Ht* cyt c_{552} and *Ne* cyt c_{552}, despite the high similarities of their three-dimensional structures to *Pa* cyt c_{551} (*22*), display axial Met conformational fluxion and heme methyl shift range compression. These two unusual cytochromes do display subtle differences in the axial Met-donating loop sequence and in heme pocket structure relative to other members of the cyt c_8 family. The NMR structure of reduced *Ne* cyt c_{552} reveals that this loop packs differently against the heme than in other members of the cyt c_8 family, perhaps as a result of the insertion of a valine after position 64 (numbering based on the *Pa* cyt c_{551}

[2] For Met, the orientation angle is determined by projecting the bisector of the Met Cγ−Sδ−Cϵ angle onto the heme plane and taking a vector perpendicular to this projection. The orientation of Met is the angle between this vector and the heme *x* axis. For His, the orientation angle is the angle between the ligand imidazole plane and the *xz* plane of the molecular coordinate system.

sequence) (*21*). Whether this structural perturbation somehow influences the Met to undergo fluxion and yield the unusual heme electronic structure remains to be determined. In the case of *Ht* cyt c_{552}, an Asn normally found at position 64 in the cyts c_8 is replaced with Gln. Asn64 is positioned to hydrogen bond with the axial Met61 in *Pa* cyt c_{551} (the Asn64 Nδ−Met61 Sδ distance is 3.61 Å in both oxidation states) (*22*). The Asn64 side chain in *Pa* cyt c_{551} also hydrogen bonds with the backbone carbonyl oxygen of Ile48 in the heme pocket. In contrast, the Gln64 side chain in *Ht* cyt c_{552} points to the periphery of the heme, toward the protein surface, and thus is not positioned to hydrogen bond with the axial Met or other heme pocket residues (*20*). Interestingly, Asn64 in the structure of *Ne* cyt c_{552}, although close to Met61, is not properly oriented to interact with the Met61 Sδ and does not engage in other hydrogen-bonding interactions within the heme pocket seen for Asn64 in *Pa* cyt c_{551} (*21*, *22*). We thus hypothesize that residue 64 plays a role in determining axial Met orientation and heme electronic structure in proteins in the cyt c_8 family. In this work, this hypothesis is tested in *Ht* cyt c_{552} by substituting Gln64 in *Ht* cyt c_{552} with Asn (yielding *Ht* Q64N). Analysis of the mutant by NMR demonstrates that this single conservative mutation drastically alters the heme methyl shift pattern from that of *Ht* cyt c_{552}, causing it to bear a remarkable resemblance to the spectrum of oxidized *Pa* cyt c_{551}. These results indicate that peripheral interactions with the axial Met play an important role in determining heme axial ligand geometry and heme electronic structure in cyts *c*.

MATERIALS AND METHODS

DNA Manipulations. Procedures were carried out generally as described in Sambrook et al. (*23*). Restriction and DNA modifying enzymes were purchased from Gibco BRL or New England Biolabs. A cloning kit for PCR products (TA cloning kit) including the pCR2.1 cloning vector was purchased from Invitrogen. *Escherichia coli* strain Nova Blue (Novagen) was used for ligation and sequencing steps. The plasmid pEC86 (*24*) was a gift from Dr. Linda Thöny-Meyer, and the plasmid pETPA (*25*) was a gift from Dr. Francesca Cutruzzolà. Oligonucleotide synthesis and DNA sequencing were performed at the Core Nucleic Acid Laboratory at the University of Rochester.

The polymerase chain reaction overlap extension method (*26*) was used to prepare the Q64N mutant of *Ht* cyt c_{552}. The pSHC$_{552}$ expression plasmid (*16*), containing the *Ht* cyt c_{552} gene preceded by an *E. coli*-compatible signal sequence, was the template. Mutagenic primers used to mutate Gln64 to Asn (underlined codon) were 5′-GCCTCCTAATAATG-TAACCGATGCG-3′ and 5′-CGGTTACATTATTAGGAG-GCATGGG-3′. The fresh PCR product was cloned into the pCR2.1 vector. Cleavage with *Bam*HI and *Nde*I removed the gene insert from the pCR2.1 vector, and the insert was cloned into pSHC552 to yield pSHC552N64 (Amp^r). The sequence of the mutant gene was confirmed by DNA sequencing. The expression plasmid pSHC552N64 and the pEC86 (Cm^r) vector [harboring cyt *c* maturation genes, *ccmABCDEFGH* (*24*)] were used to transform BL21(DE3)-Star competent cells to chloramphenicol and ampicillin resistance.

Protein Expression and Purification. Expression of *Ht* Q64N was achieved by growing BL21(DE3)Star cells containing the pSHC552N64 plasmid in LB medium supplemented with ampicillin (50 μg/mL) and chloramphenicol (50 μg/mL). The culture was agitated at 140 rpm at 37 °C for 16 h. *Ht* cyt c_{552} was expressed in BL21(DE3) cells harboring pSHC552 and pEC86. Cells were harvested by centrifugation. Purification of wild-type and mutant *Ht* cytochromes from cell pellets was as described in detail for *Ht* cyt c_{552} (*16*). *Pa* cyt c_{551} was expressed and purified as described (*25*). Horse heart cyt *c* was obtained from Sigma.

NMR Spectroscopy. ^{1}H NMR spectra were collected on a Varian INOVA 500 MHz spectrometer. Data were collected on samples (2−3 mM) of *Ht* Q64N (oxidized and reduced) in 120 mM sodium acetate-d_3, pH 5.0, with 10% D_2O. The temperature was 300 K unless indicated otherwise. Oxidized samples contained a 5-fold molar excess of $K_3[Fe(CN)_6]$, and reduced samples contained a 20−30-fold molar excess of $Na_2S_2O_4$. Samples were deoxygenated by bubbling nitrogen gas before addition of $Na_2S_2O_4$. For oxidized *Ht* Q64N, 2-D NOESY (mixing time 100 ms) and TOCSY (spin-lock time 50 ms) spectra were collected with 8192 points in the F_2 dimension, 512 increments in the F_1 dimension, and a 30000 Hz spectral width. For reduced protein, NOESY (mixing time 100 ms) and TOCSY (spin-lock time 90 ms) spectra had 4096 points in the F_2 dimension and 512 points in the F_1 dimension and a 12000 Hz spectral width. NMR data processing and analysis were performed using FELIX 97 (MSI). For variable temperature (268−300 K) experiments, samples with 20% (v/v) CD_3OD were used.

NMR Data Analysis. Heme ^{1}H resonances of oxidized and reduced *Ht* Q64N were assigned by identifying connectivities between heme substituents in NOESY spectra. Assignments were confirmed by identifying NOEs between heme substituents and nearby amino acid side chains. Assignments of proton resonances for heme pocket amino acids were made using standard procedures (*27*) and assisted by comparison to published assignments for *Ht* cyt c_{552} (*16*, *20*).

Experimental pseudocontact shifts (δ_{pc}^{obs}) for *Ht* Q64N were determined by taking the difference between the shift of a proton in the oxidized (δ_{ox}) and reduced (δ_{red}) states:

$$\delta_{pc}^{obs} = \delta_{para} - \delta_{dia} = \delta_{ox} - \delta_{red} \quad (1)$$

This relationship assumes a contact shift of zero, which is valid for protons not on the heme or axial ligands (*10*), and no redox-linked structure change, which is valid for most nuclei in cyts *c* (*22*, *28*, *29*). The orientation of the magnetic axes and the values of the axial ($\Delta\chi_{ax}$) and rhombic ($\Delta\chi_{rh}$) anisotropies for oxidized *Ht* Q64N were determined from experimental pseudocontact shift data (Table S1) as described in detail elsewhere (*5*). Fitting was done to eq 2, in which r', θ', and Ω' are the positions of the nucleus in the molecular coordinate system and $R(\alpha, \beta, \gamma)$ is the Eulerian rotation matrix transforming the molecular to the magnetic coordinates r, θ, Ω (*10*, *30*):

$$\delta_{pc} = ({}^1/_{12}\pi r'^3)[\Delta\chi_{ax}(3\cos^2\theta' - 1) + {}^3/_2\Delta\chi_{rh}(\sin^2\theta' \cos 2\Omega')][R(\alpha, \beta, \gamma)] \quad (2)$$

The first structure of the family of structures for *Ht* cyt c_{552}, determined by NMR (*20*), was used in the magnetic axes search. Shifts for the mutated residue 64 were not included.

CD and UV−Vis Spectroscopy. Circular dichroism (CD) spectra were collected on a JASCO J-710 spectropolarimeter at ambient temperature (298 K). Oxidized protein samples (1−3 mM) were in 50 mM sodium phosphate, pH 7.0, in a 0.100 cm path length quartz cell. Four scans at 200 nm/min with a 2 s response time and 2 or 5 mdeg sensitivity were collected for each sample from 615 to 725 nm at a 0.5-nm step resolution.

Absorption measurements were made on a Shimadzu UV-2401PC photometer unit at ambient temperature. Spectra were collected of both the oxidized (as purified) and reduced (small excess of dithionite added) species. Extinction coefficients of 105000 L mol^{-1} cm^{-1} at 409.5 nm [*Ht* cyt c_{552} (*16*)], 106500 L mol^{-1} cm^{-1} at 410 nm [*Pa* cyt c_{551} (*31*)], and 106100 L mol^{-1} cm^{-1} [horse heart cyt *c* (*32*)] were used to determine protein concentrations.

RESULTS AND DISCUSSION

Protein Expression. The yield of *Ht* Q64N was 1.2 μmol of protein/L of culture, which is similar to the yield for wild-type protein (*16*). *Ht* Q64N displayed the same chromatographic profile as reported for wild type (*16*). The UV−vis absorption spectrum of oxidized *Ht* Q64N was indistinguishable from that of wild-type *Ht* cyt c_{552} (*16*), including the presence of a weak absorption band at ~690 nm, indicative of Met ligation (*33*). The bands in reduced *Ht* Q64N display 0.5−1.0 nm shifts relative to wild type, although this difference is only marginally outside the wavelength accuracy of the instrument [±0.3 nm; λ_{max} = 415.5, 521.0, and 550.5 nm for *Ht* Q64N; compare to 416.0, 520.0, and 552.0 nm for wild type (*16*)]. The 550.5 nm band for *Ht* Q64N (the α or Q_{00} band) displays the expected splitting, suggesting that the heme in the mutant deviates from planarity, as is seen for wild type and is typical for cyts *c* (*16*, *34*, *35*). Expression of *Pa* cyt c_{551} (*25*) and of wild-type *Ht* cyt c_{552} (*16*) gave products with chromatographic properties and absorption spectra the same as those previously described.

Heme Resonance Assignments. The downfield region of the ^{1}H NMR spectrum of oxidized *Ht* Q64N is shown in Figure 2D. A dramatic change in hyperfine shifts relative to wild-type *Ht* cyt c_{552} (Figure 2C) (*16*) is caused by this mutation. Selected heme proton chemical shifts for *Ht* Q64N are listed in Table 1, along with shifts for *Ht* cyt c_{552} and *Pa* cyt c_{551} for comparison. The Q64N mutation changes the ordering of heme methyl shifts in *Ht* cyt c_{552} from the pattern of 8-CH_3 > 5-CH_3 ~ 3-CH_3 > 1-CH_3 seen in wild type to 5-CH_3 > 1-CH_3 > 8-CH_3 > 3-CH_3, which is the pattern observed for oxidized *Pa* cyt c_{551}. In addition, the spread of the heme methyl shifts increases from 6.12 to 19.52 ppm (300 K). The shift values of all heme substituents in oxidized *Ht* Q64N are remarkably similar to those of oxidized wild-type *Pa* cyt c_{551} (*14*, *36*), suggesting similar heme electronic structures (Table 1).

Assignments of heme substituent resonances in diamagnetic, reduced *Ht* Q64N also are listed in Table 1. The chemical shifts in the diamagnetic protein serve as a useful indicator of any structure change that occurred as a result of mutation. The similarity between the heme substituent chemical shifts of reduced *Ht* Q64N and wild-type *Ht* cyt c_{552} (*16*) suggests that the conformation of the heme itself is not changed significantly by the mutation. This observation suggests that the dramatic change in chemical shifts in the oxidized form of *Ht* Q64N relative to wild type is a result of a perturbation of one or both of the axial ligands to the heme.

Table 1: Chemical Shifts of Selected ^{1}H Resonances of Heme, the Axial Met61, and Residue 64 in Wild-Type and Mutant Cytochromes *c*[a]

	Ht cyt c_{552}[b]		*Ht* Q64N[c]		*Pa* cyt c_{551}	
substituent	Fe(III)	Fe(II)	Fe(III)	Fe(II)	Fe(III)[d]	Fe(II)[e]
1-CH_3	18.16	3.68	26.57	3.67	26.53	3.69
3-CH_3	22.29	3.87	12.90	3.88	13.17	3.75
5-CH_3	22.89	3.32	32.42	3.35	31.51	3.31
8-CH_3	24.28	3.45	17.32	3.52	15.99	3.40
α-*meso*-H	1.54	9.80	8.50	10.01	8.89	9.85
β-*meso*-H	−0.42	9.37	−0.48	9.42	−1.32	9.37
γ-*meso*-H	9.07	9.42	6.54	9.44	6.66	9.36
δ-*meso*-H	−1.17	9.28	−2.53	9.30	−3.08	9.23
Met61 Hγ1	−12.8	−1.08	−10.4	−0.55	−8.0	−0.50
Met61 Hγ2	−20.2	−3.36	−34.1	−3.62	−40.8	−3.50
Met61 ϵ-CH_3	−17.2	−2.89	−14.5	−2.97	−17.1	−2.92
Asn/Gln64 HNδ/ϵ1[f]	8.81	6.37	12.68	3.18	13.46	3.18
Asn/Gln64 HNδ/ϵ2[f]	6.70	6.67	13.78	7.50	13.86	7.58

[a] Shifts are in ppm and are measured at 300 K. Samples are in 120 mM sodium acetate-d_3, pH 5, unless noted otherwise. Oxidized protein samples contain a 5-fold molar excess of $K_3[Fe(CN)_6]$, and reduced samples contain a 20−30-fold excess of $Na_2S_2O_4$. [b] Assignments are from ref *16*. Assignments for reduced protein were previously reported in ref *20*. [c] This work. [d] 50 mM sodium phosphate, pH 6.0. Assignments are from ref *25*. Assignments were previously reported in ref *36*. [e] Shifts are from ref *5*; assignments were previously reported in refs *36*, *42*, and *49*. [f] HNδ1 for Asn64 in *Pa* cyt c_{551} and in *Ht* Q64N is defined as the proton closer to the axial Met Sδ. HNϵ2 for Gln64 in *Ht* cyt c_{552} is defined as the proton closer to the heme 3-CH_3.

Orientation of the Axial His. The heme methyl shift pattern observed for *Ht* Q64N (Figure 2D) represents a dramatic change from that seen for wild type (Figure 2C, Table 1). In the absence of heme modification, a dramatic change in oxidized heme shifts in a protein variant can be a result of perturbing the interactions between the heme and one or both axial ligands. This analysis will focus on the axial Met because it is not expected that the axial His would be affected significantly by this mutation. Cytochromes *c* generally have their axial His aligned along the α−*γ*-*meso* axis of the heme, regardless of species. Conservation of this alignment is likely a result of local bonding constraints (in particular, the Cys-X-Y-Cys-His heme-binding motif) determining axial His orientation in cyts *c*. Indeed, it has been shown that cyt *c* heme peptide fragments (microperoxidases) retain a native-like axial His orientation (*37*, *38*). Also, it has been demonstrated spectroscopically that *Ht* cyt c_{552} and *Pa* cyt c_{551} have the same axial His orientation, despite their differing hyperfine shifts (*39*). Finally, similarity of the chemical shifts of His16 in reduced *Ht* Q64N and in wild type supports the assumption that the His is not perturbed by mutation: The chemical shifts of the His16 side chain in *Ht* Q64N [and in wild-type *Ht* cyt c_{552} (*16*)] are Hβ1, 0.78 (0.72); Hβ2, −0.14 (−0.17); HNδ1, 8.96 (8.95); Hϵ1, 0.65 (0.63); and Hδ2, 0.90 ppm (0.79 ppm).

Analysis of Axial Met Orientation in Reduced Ht Q64N. Axial Met ligands are found in a number of conformations in *c*-type cytochromes, depending on the species (*10*, *14*). The two most common are shown in Figure 1 (both conformations superimposed in Figure 1A). The X-ray crystal structure indicates that *Pa* cyt c_{551} has the Met orientation

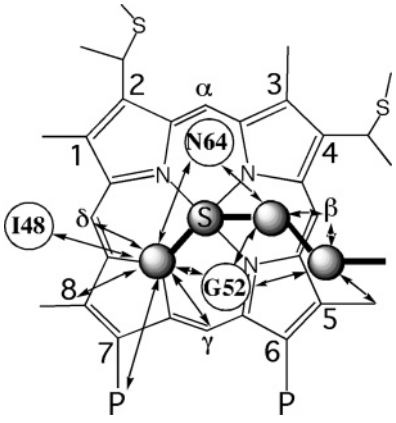

FIGURE 4: NOEs observed between Met61 ϵ-CH_3 and heme substituents in reduced *Ht* Q64N.

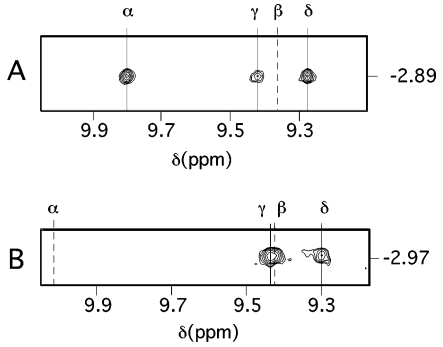

FIGURE 5: Cross-peaks between heme *meso* protons (labeled α, *β*, *γ*, *δ*) and the axial Met61 ϵ-CH_3 in NOESY spectra of reduced (A) *Ht* cyt c_{552} and (B) *Ht* Q64N. The dotted lines indicate the chemical shifts of heme *meso* protons that do not show cross-peaks with Met61 ϵ-CH_3.

shown in Figure 1B, with the Met61 ϵ-CH_3 directed toward heme pyrrole III and *S* chirality at Met sulfur (*22*). NMR analysis of reduced *Ht* cyt c_{552} suggests that the axial Met is sampling two orientations as shown in Figure 1A. One of these orientations is proposed to be similar to that typically seen in mitochondrial cyts *c* with the Met61 ϵ-CH_3 oriented toward the heme pyrrole I nitrogen and *R* chirality at the sulfur (*R* conformation in Figure 1A) (*20*), and the other is proposed to be similar to the orientation in *Pa* cyt c_{551} (*5*). NMR determination of the axial Met conformation is based on analysis of NOEs between the Met and the heme, which show a distinctive pattern according to the Met conformation (*15*). Analysis of the *Pa* cyt c_{551} crystal structure indicates that strong NOESY cross-peaks are expected between the axial Met ϵ-CH_3 and the heme *γ*-*meso*-H and *δ*-*meso*-H for Met in the conformation in Figure 1B. Of the heme methyls, 8-CH_3 is closest to Met61 ϵ-CH_3 in *Pa* cyt c_{551}. Cyts *c* with Met oriented as in the mitochondrial cyts *c*, or in orientation *R* in Figure 1A, however, have axial Met ϵ-CH_3 in proximity of the heme α-*meso*-H and *δ*-*meso*-H, as well as the 2-thioether-H. NOEs are not expected from the axial Met ϵ-CH_3 to the *γ*-*meso*-H or 8-CH_3 in that case (*40*, *41*). For both orientations, NOEs between the Met H*γ*12 and the heme *β*-*meso*-H are expected as well.

The NOESY spectrum of reduced *Ht* Q64N thus was analyzed to identify NOEs that define the orientation of the axial Met. NOESY cross-peaks between the heme and axial ligands are more reliably detected and interpreted in the diamagnetic, reduced form of cyt *c* than in the oxidized state in which heme paramagnetism severely attenuates NOESY peak intensity. (It is important to note, however, that differences in Met orientation and the nature of any conformational dynamics between the two oxidation states are possible.) Assignment of the Met61 resonances in reduced *Ht* Q64N was achieved by identification of the characteristic upfield-shifted (by heme ring current) resonances with intraresidue TOCSY cross-peaks consistent with a Met (HN, 8.39; Hα, 3.63; H*β*, −0.81, −2.78; H*γ*, −0.55, −3.62; ϵ-CH_3, −2.97 ppm). The NOEs detected from the Met61 side chain to the heme and to nearby heme pocket residues in *Ht* Q64N are illustrated with arrows in Figure 4, and cross-peaks between the Met61 ϵ-CH_3 and the heme *meso* protons in *Ht* Q64N and in *Ht* cyt c_{552} are shown in Figure 5. The Met61 ϵ-CH_3 displays NOEs of similar intensities to the heme *δ*- and *γ*-*meso*-H, a strong cross-peak with the heme 8-CH_3, and a medium-intensity cross-peak with the heme 7-propionate-Hα. In addition, a NOESY cross-peak between the *β*-*meso*-H and Met61 H*γ* was detected. This pattern is strikingly similar to that seen for *Pa* cyt c_{551} (*5*, *15*), suggesting similar Met orientations in reduced *Pa* cyt c_{551} and in *Ht* Q64N. These results contrast with observations for wild-type *Ht* cyt c_{552}, in which the above NOEs seen for the mutant in addition to NOEs from Met61 ϵ-CH_3 to the α-*meso*-H and 2-thioether-H, characteristic of the "eukaryotic" conformation of the Met (*20*, *40*, *41*), were observed (*5*). The absence of these latter connectivities in *Ht* Q64N suggests that the Q64N mutation suppresses motion of the axial Met seen in wild type. The NOEs from Met61 in reduced *Ht* Q64N thus indicate that the axial Met has a single major orientation that is similar to that observed for *Pa* cyt c_{551}.

Analysis of Axial Met Orientation in Oxidized Ht Q64N. The striking similarity of the hyperfine shift patterns for oxidized *Ht* Q64N and *Pa* cyt c_{551} is suggestive of similar axial ligand−heme interactions (*13*). Assuming that the axial His has similar orientations in *Ht* Q64N and *Pa* cyt c_{551}, it follows that the difference in heme methyl shifts seen between wild type and *Ht* Q64N indicates a change in the axial Met, with the Met taking a conformation similar to that for *Pa* cyt c_{551} in *Ht* Q64N. This conclusion is in agreement with conclusions from analysis of reduced *Ht* Q64N.

The orientation of the magnetic axes determined for *Ht* Q64N also provides an indication of the axial ligand orientations. The fitting procedure provides information on the orientation of the magnetic axes relative to the molecular axes in terms of three Euler angles (α, *β*, *γ*) of rotation (*30*) (Figure 6). A plot of the resulting calculated and experimental pseudocontact shifts is shown as Supporting Information (Figure S1). The angle *β* (−10° for *Ht* Q64N) is the tilt of the magnetic *z* axis from the heme normal, and because this value is small, the quantity $\alpha + \gamma$ indicates the in-plane rotation of the magnetic axes relative to the molecular axes, *κ*. The relationship between the magnetic axes orientation and the axial ligand orientations is provided by the "counterrotation rule" (*10*, *18*, *19*). In this formalism, if the mean axial ligand plane is oriented at an angle Φ from a N−Fe−N axis in the heme plane, the direction of the minimum *χ* value (χ_{xx}) would be at an angle $\kappa = -\Phi$ from that same axis (Figure 6) (*10*, *18*, *19*). In *Pa* cyt c_{551}, the value of Φ measured from its crystal structure is 16°, which predicts a

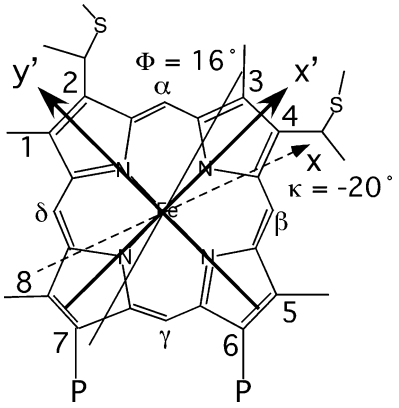

FIGURE 6: Orientation of magnetic axes in *Ht* Q64N. The solid line indicates the mean of the His and Met orientation angles, and the dashed line indicates κ, which is the orientation of χ_{xx}. The parameters determined in the fit are $\alpha = 35°$, $\beta = -10°$, $\kappa = -20°$, $\Delta\chi_{ax} = 3.30 \times 10^{-32}$ m^3, and $\Delta\chi_{rh} = -0.92 \times 10^{-32}$ m^3.

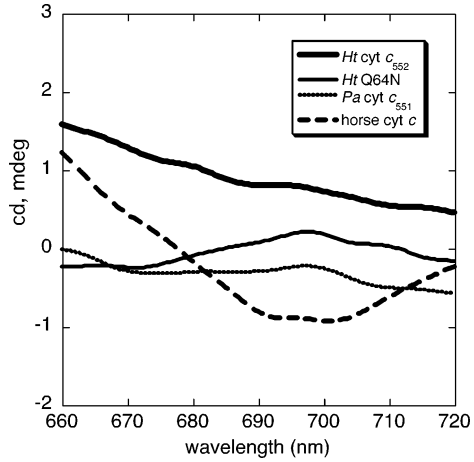

FIGURE 7: CD spectra of oxidized *Ht* cyt c_{552} (2.6 mM, thick solid line), *Ht* Q64N (1.8 mM, thin solid line), *Pa* cyt c_{551} (1.5 mM, dotted line), and horse cyt *c* (1.1 mM, dashed line).

κ value of $-16°$. Our measured κ value for *Ht* Q64N is $-20°$, which is in reasonable agreement. Notably, this is a large change from the κ for *Ht* cyt c_{552} of $-47°$, which is consistent with conformational averaging of the Met (*5*).

In addition to the heme resonance shifts and magnetic axes, another indication that the axial Met is sampling more than one conformation was the line broadening observed for all four heme methyls of *Ht* cyt c_{552} at low temperature. This line broadening was found to be independent of T_1, supporting the proposal that a chemical exchange process is responsible for the increased line widths. In contrast to *Ht* cyt c_{552}, *Pa* cyt c_{551} does not display significant line broadening at low temperature (*5*). To verify that *Ht* Q64N does not undergo axial Met conformational exchange, its NMR spectrum was collected at 268 K. The line widths of the *Ht* Q64N heme methyls at 268 K are similar to those of *Pa* cyt c_{551}; i.e., the line broadening observed for wild type is not present for the mutant (Figure S2, Supporting Information). This observation supports the proposal that the axial Met in *Ht* Q64N is not fluxional but rather occupies a conformation similar to that in *Pa* cyt c_{551}.

An independent measure of the axial Met configuration at sulfur can be obtained by the CD spectrum in the region of the 690 nm band, which is indicative of Met−Fe(III) ligation. A positive Cotton effect in this region indicates *S*-chirality at the Met ligand sulfur and a negative Cotton effect *R*-chirality (*15*). The CD spectrum of oxidized horse cyt *c*, for example, shows a negative Cotton effect, whereas that of *Pa* cyt c_{551} shows a positive Cotton effect (Figure 7). The spectrum of *Ht* cyt c_{552} does not show any distinct band in this region, a finding consistent with, although not proof of, the proposed Met dynamics. *Ht* Q64N, in contrast, shows a positive band, consistent with the proposal that it exhibits *S* chirality as does *Pa* cyt c_{551}.

Analysis of Residue 64 Conformation. Assignments of Asn64 resonances in reduced *Ht* Q64N were made by identifying sequential NOESY connectivities from Asn64 to Asn65 (64HN−65HN, 64Hβ−65HN). The chemical shifts of HNδ1 and HNδ2 in reduced *Ht* Q64N are 3.18 and 7.50 ppm, respectively. The HNδ1 proton is defined here as the proton closer to the Met Sδ and is identified by its medium-to-strong NOEs with Met61 ϵ-CH_3 and Hγ2, whereas HNδ2 has NOEs with Ile48 side chain protons and heme 2-CH_3. The unusual chemical shift of 3.18 ppm indicates that HNδ1 is shifted upfield by the heme ring current, consistent with a position near the axial Met Sδ. The shifts of the Asn HNδ12 in *Ht* Q64N are remarkably similar to those measured for Asn64 HNδ12 in reduced *Pa* cyt c_{551} [3.18, 7.58 ppm (*42*); Table 1]. The similar, unusual shift of 3.18 ppm for the Asn64 HNδ1 in *Ht* Q64N and in *Pa* cyt c_{551} indicates that this residue experiences a similar ring current shift in both proteins (no other aromatic groups are near residue 64 in either protein). In the crystal structure of *Pa* cyt c_{551}, the Asn64 side chain is positioned to hydrogen bond with Met61 Sδ, and these data support a similar interaction existing in *Ht* Q64N. The NOEs reported above for the Asn64 in *Ht* Q64N are the same as are observed for reduced *Pa* cyt c_{551} (NOEs found in assignment of *Pa* cyt c_{551} in ref *5*) and thus are consistent with an Asn64 position in *Ht* Q64N similar to that seen for *Pa* cyt c_{551} (Figure 1B) (*22*).

In contrast with *Pa* cyt c_{551} and *Ht* Q64N, residue 64 (Gln) in wild-type *Ht* cyt c_{552} does not show a downfield ring current shift for either HNϵ12 proton (6.37, 6.68 ppm) (*16*, *20*). The Gln64 HNϵ12 protons also display a different pattern of NOEs than do the Asn64 HNδ12 in *Ht* Q64N. In *Ht* cyt c_{552}, both have NOEs with the heme 3-CH_3, Pro62 Hγ and Hβ, and Met61 ϵ-CH_3. Unlike residue 64 in *Pa* cyt c_{551} and in *Ht* Q64N, NOEs to Ile48 are not observed for the Gln64 HNϵ12 protons. These data are in agreement with the NMR structure of *Ht* cyt c_{552} in which Gln64 occupies a different position than does Asn64 in *Pa* cyt c_{551} (Figure 1).

Sequence-specific assignments of proton resonances for Asn64 in oxidized *Ht* Q64N were made by identification of the expected sequential NOEs between Pro63, Asn64, and Asn65. In oxidized *Ht* Q64N, the HNδ2 (13.78 ppm) is identified by its NOEs with the Ile48 side chain and heme 2-CH_3, as well as an NOE to a proton at 12.68 ppm, assigned as N64 HNδ1. The HNδ1 proton does not display any interresidue NOEs, which is attributed to efficient relaxation enhancement by the paramagnetic heme. These chemical shifts are similar to those reported for oxidized *Pa* cyt c_{551} Asn64 (HNδ1, 13.46; HNδ2, 13.86) (*25*). The unusual chemical shifts for these protons are attributed to a significant pseudocontact contribution to the shift. According to eq 1, the experimental pseudocontact shifts for the Asn64 HNδ12 protons in *Ht* Q64N are 10.28 (HNδ1) and 6.28 ppm (HNδ2).

The expected pseudocontact shifts for these protons in *Ht* Q64N, assuming the Asn64 position is the same relative to the heme as in *Pa* cyt c_{551}, and no contact contribution to the shift, can be calculated according to eq 2 using the parameters determined in the magnetic axes search (Figure 6). The resulting calculated pseudocontact shifts for the Asn64 HNδ12 protons in *Ht* Q64N are 10.66 (HNδ1) and 7.01 ppm (HNδ2). The similarities between these calculated values, based on the Asn64 position reported in the *Pa* cyt c_{551} crystal structure, and the experimental values for *Ht* Q64N strongly support the proposal that the position of Asn64 in oxidized *Ht* Q64N is similar to that seen in *Pa* cyt c_{551}.

Determinants of Axial Met Fluxion. *Ht* Q64N displays a remarkable resemblance to *Pa* cyt c_{551} in a number of respects. One is the heme methyl hyperfine shifts, which indicate similar unpaired electron spin distributions and thus similar axial ligand orientations relative to the heme. Second, the orientations of the magnetic axes of *Ht* Q64N and *Pa* cyt c_{551} are similar, also suggesting similar heme−ligand interactions. The NOEs from the axial Met to the heme in the reduced proteins also indicate a similar Met orientation. Finally, the NMR chemical shifts of Asn64 are remarkably similar in these proteins. Notably, these shifts are determined by both the placement of Asn relative to the heme and, in the oxidized forms, the magnetic axes orientation and magnetic anisotropy of the heme. These data support the hypothesis that mutating Gln64 to Asn in *Ht* cyt c_{552} stops the Met fluxion, freezing the axial Met into the *S* configuration seen in *Pa* cyt c_{551}. This analysis, however, does not answer the question as to why the Met undergoes fluxion in wild-type *Ht* cyt c_{552}. We raise two hypotheses. One is that the fluxion arises from strain experienced by the iron−Met interaction in *Ht* cyt c_{552}. The strain raises ground state energy to allow access to the transition state for Met sulfur inversion, in analogy to other molecules that undergo inversion at sulfur (*4*, *43*). Indeed, molecules undergoing inversion at sulfur-based ligands generally show strain or steric crowding (*4*). The highly rigid nature of the Met-donating loop in the cyts c_8 may contribute to this behavior in some cases (*5*, *25*). The suppression of the fluxion in *Ht* Q64N then results from stabilizing one fixed state by introducing favorable interactions between Asn64 and Met61, assisted by Asn64−Ile48 interactions as well. The other hypothesis is that the intrinsic barrier for Met rearrangement is low, and a Met ligand will undergo fluxion as long as groups are not present to block it. In other words, the dynamics exhibited by the axial Met in *Ht* cyt c_{552} represents the "default" case, and the fluxion is not present in *Pa* cyt c_{551}, and in most cyts *c*, because a heme pocket residue blocks the motion. Additional studies of a range of cyt *c* variants are required to determine the origin of this interesting fluxional behavior, as well as its consequences for protein stability and for electron transfer activity.

Peripheral Interactions with Axial Met in Other Cytochromes c. Efficient expression systems capable of producing a range of holocytochromes *c* have become available relatively recently (*16*, *24*, *35*, *44*, *45*). Thus, there are few reports of how mutations of residues that interact with axial ligands affect cyt *c* properties. One exception is *Saccharomyces cerevisiae* iso-1-cyt *c* (*Sc* cyt *c*). In *Sc* cyt *c* as in other mitochondrial cyts *c*, a strongly conserved Tyr at position 67 is known to hydrogen bond with the axial Met80 Sδ. The Y67F mutant of *Sc* cyt *c*, made to remove this hydrogen-bonding interaction, has been characterized extensively. Electrochemical characterization of this mutant indicates that this interaction plays a role in regulating redox potential. The crystal structure of *Sc* Y67F, however, indicates a Met conformation similar to that of wild-type protein (*46*). (NMR data on oxidized *Sc* Y67F, however, have not been reported.) Other position 67 mutants (Y67R, Y67K) were found to be nonfunctional (i.e., they could not be expressed in *S. cerevisiae*) (*47*).

Other information on peripheral interactions with cyt *c* heme ligands comes from analysis of native proteins. A cyt *c* particularly relevant to this work is *Ne* cyt c_{552}. The three-dimensional structure and axial Met conformation in reduced *Ne* cyt c_{552} have been determined by NMR and are reported to be similar to *Pa* cyt c_{551} (*21*). NMR analysis of oxidized *Ne* cyt c_{552}, however, suggests the presence of axial Met dynamics as is seen in *Ht* cyt c_{552}, despite the apparently fixed position of the axial Met in reduced *Ne* cyt c_{552} (*6*). Interestingly, an Asn is present at position 64 in *Ne* cyt c_{552}, but the structure of *Ne* cyt c_{552} reveals that the packing on the axial Met side of the heme is perturbed relative to that seen for *Pa* cyt c_{551}. Asn64, although close to the axial Met (Asn Nδ−Met Sδ distance of 3.27 Å), is positioned differently from Asn64 in *Pa* cyt c_{551}. In particular, it lacks hydrogen-bonding interactions with the backbone carbonyls of residues Ile48 and Lys49 that are present in *Pa* cyt c_{551} (*22*). The perturbation of the heme pocket structure in *Ne* cyt c_{552} may be a result of a sequence insertion in the loop containing this residue, after residue 64 (*21*). Additional studies of the molecular and electronic structures of *Ne* and *Ht* cyts c_{552} are required to understand the determinants of Met conformation and heme electronic structure, as well as implications of electronic structure variation for electron transfer function (*48*). In particular, variants such as *Ht* Q64N with altered electronic structures are expected to be excellent systems for investigating the effect of heme electronic structure on electron transfer activity.

ACKNOWLEDGMENT

The authors thank Linda Thöny-Meyer for the gift of pEC86 and Francesca Cutruzzolà and Maria Giulia Bigotti for pETPA. We thank Brandy Russell for helpful discussions and Ravinder Kaur for assistance with analysis of cyt *c* structures.

SUPPORTING INFORMATION AVAILABLE

Table of experimental and calculated pseudocontact shifts for *Ht* Q64N (Table S1), plot of calculated vs experimental pseudocontact shifts for *Ht* Q64N (Figure S1), and ^{1}H NMR spectra of *Pa* cyt c_{551}, *Ht* cyt c_{552}, and *Ht* Q64N at 268 and 300 K (Figure S2). This material is available free of charge via the Internet at http://pubs.acs.org.

REFERENCES

1. Que, L., and Tolman, W. B. (2004) Recurring structural motifs in bioinorganic chemistry, in *Comprehensive Coordination Chemistry II* (McCleverty, J. A., and Meyer, T. J., Eds.) Vol. 8, pp 1−15, Elsevier, Berlin.
2. Winkler, J. R., Wittung-Stafshede, P., Leckner, J., Malmström, B. G., and Gray, H. B. (1997) Effects of folding on metalloprotein active sites, *Proc. Natl. Acad. Sci. U.S.A. 94*, 4246−4249.

3. Cotton, F. A., Wilkinson, G., Murillo, C. A., and Bochmann, M. (1999) *Advanced Inorganic Chemistry*, 6th ed., pp 13−24, Wiley, New York.
4. Toyota, S. (1999) Mechanisms of inversion at pyramidal sulfur atoms in three-coordinate sulfur compounds, *Rev. Heteroat. Chem. 21*, 139−162.
5. Zhong, L., Wen, X., Rabinowitz, T. M., Russell, B. S., Karan, E. F., and Bren, K. L. (2004) Heme axial methionine fluxionality in *Hydrogenobacter thermophilus* cytochrome c_{552}, *Proc. Natl. Acad. Sci. U.S.A. 101*, 8637−8642.
6. Bren, K. L., Kellogg, J. A., Kaur, R., and Wen, X. (2004) Folding, conformational changes, and dynamics of cytochromes *c* probed by NMR spectroscopy, *Inorg. Chem. 43*, 12162−12176.
7. Scott, R. A., and Mauk, A. G. (1996) *Cytochrome c: A Multidisciplinary Approach*, University Science Books, Sausalito, CA.
8. Moore, G. R., and Pettigrew, G. W. (1990) *Cytochrome c: Evolutionary, Structural and Physicochemical Aspects*, Springer-Verlag, New York.
9. Lee, K.-B., La Mar, G. N., Mansfield, K. E., Smith, K. M., Pochapsky, T. C., and Sligar, S. G. (1993) Interpretation of hyperfine shift patterns in ferricytochrome *b*(5) in terms of angular position of the heme—a sensitive probe for peripheral heme protein interactions, *Biochim. Biophys. Acta 1202*, 189−199.
10. LaMar, G. N., Satterlee, J. D., and deRopp, J. S. (2000) Nuclear magnetic resonance of hemoproteins, in *The Porphyrin Handbook* (Kadish, K. M., Smith, K. M., and Ruilard, R., Eds.) Vol. 5, pp 185−298, Academic Press, New York.
11. Kurland, R. J., and McGarvey, B. R. (1970) Isotropic NMR shifts in transition metal complexes: The calculation of the Fermi contact and pseudocontact terms, *J. Magn. Reson. 2*, 286−301.
12. Bertini, I., and Luchinat, C. (1996) NMR of paramagnetic substances, *Coord. Chem. Rev. 150*, 29−75.
13. Shokhirev, N. V., and Walker, F. A. (1998) The effect of axial ligand plane orientation on the contact and pseudocontact shifts of low-spin ferriheme proteins, *J. Biol. Inorg. Chem. 3*, 581−594.
14. Senn, H., and Wüthrich, K. (1985) Amino acid sequence, heme-iron coordination geometry and functional properties of mitochondrial and bacterial *c*-type cytochromes, *Q. Rev. Biophys. 18*, 111−134.
15. Senn, H., Keller, R. M., and Wüthrich, K. (1980) Difference in the chirality of the axial methionine in homologous cytochromes *c* determined by H-1-NMR and CD spectroscopy, *Biochem. Biophys. Res. Commun. 92*, 1362−1369.
16. Karan, E. F., Russell, B. S., and Bren, K. L. (2002) Characterization of *Hydrogenobacter thermophilus* cytochromes *c*(552) expressed in the cytoplasm and periplasm of *Escherichia coli*, *J. Biol. Inorg. Chem. 7*, 260−272.
17. Timkovich, R., Cai, M., Zhang, B., Arciero, D. M., and Hooper, A. B. (1994) Characteristics of the paramagnetic H-1-NMR spectra of the ferricytochrome *c*-551 family, *Eur. J. Biochem. 226*, 159−168.
18. Shokhirev, N. V., and Walker, F. A. (1998) Co- and counterrotation of magnetic axes and axial ligands in low-spin ferriheme systems, *J. Am. Chem. Soc. 120*, 981−990.
19. Turner, D. L. (1995) Determination of heme electronic structure in His-Met cytochromes *c* by C-13 NMR—The effect of the axial ligands, *Eur. J. Biochem. 227*, 829−837.
20. Hasegawa, J., Yoshida, T., Yamazaki, Y., Sambongi, Y., Yu, Y., Igarashi, Y., Kodama, T., Yamazaki, K., Kyogoku, Y., and Kobayashi, Y. (1998) Solution structure of thermostable cytochrome *c*-552 from *Hydrogenobacter thermophilus* determined by ^{1}H NMR spectroscopy, *Biochemistry 37*, 9641−9649.
21. Timkovich, R., Bergmann, D., Arciero, D. M., and Hooper, A. B. (1998) Primary sequence and solution conformation of ferrocytochrome *c*-552 from *Nitrosomonas europaea*, *Biophys. J. 75*, 1964−1972.
22. Matsuura, Y., Takano, T., and Dickerson, R. E. (1982) Structure of cytochrome *c*551 from *Pseudomonas aeruginosa* refined at 1.6 Å resolution and comparison of the 2 redox forms, *J. Mol Biol. 156*, 389−409.
23. Sambrook, J., Fritsch, E. F., and Manaiatis, T. (1989) *Molecular Cloning*: *A Laboratory Manual*, 2nd ed., Cold Spring Harbor Laboratory Press, New York.
24. Arslan, E., Schulz, H., Zufferey, R., Künzler, P., and Thöny-Meyer, L. (1998) Overproduction of the *Bradyrhizobium japonicum c*-type cytochrome subunits of the *cbb*(3) oxidase in *Escherichia coli*, *Biochem. Biophys. Res. Commun. 251*, 744−747.
25. Russell, B. S., Zhong, L., Bigotti, M. G., Cutruzzolà, F., and Bren, K. L. (2002) Backbone dynamics and hydrogen exchange of oxidized *Pseudomonas aeruginosa* ferricytochrome c_{551}, *J. Biol. Inorg. Chem. 8*, 156−166.
26. Ho, S. N., Hunt, H. D., Horton, R. M., Pullen, J. K., and Pease, L. R. (1989) Site-directed mutagenesis by overlap extension using the polymerase chain reaction, *Gene 77*, 51−59.
27. Wüthrich, K. (1986) *NMR of Proteins and Nucleic Acids*, Wiley, New York.
28. Scheijter, A. (1996) Oxidation state-dependent properties of cytochromes *c*, in *Cytochrome c: A Multidisciplinary Approach* (Scott, R. A., and Mauk, A. G., Eds.) pp 335−345, University Science Books, Mill Valley, CA.
29. Berghuis, A. M., and Brayer, G. D. (1992) Oxidation state-dependent conformational changes in cytochrome *c*, *J. Mol. Biol. 223*, 959−976.
30. Emerson, S. D., and La Mar, G. N. (1990) NMR determination of the orientation of the magnetic susceptibility tensor in cyanometmyoglobin: A new probe of steric tilt of bound ligand, *Biochemistry 29*, 1556−1566.
31. Horio, T., Higashi, T., Sasagawa, M., Kusai, K., Nakai, M., and Okunuki, K. (1960) Preparation of crystalline *Pseudomonas* cytochrome *c*-551 and its general properties, *Biochem. J. 77*, 194−201.
32. Margoliash, E., and Frohwirt, N. (1959) Spectrum of horse heart cytochrome *c*, *Biochem. J. 71*, 570−572.
33. Harbury, H. A., Cronin, J. R., Fanger, M. W., Hettinger, T. P., Murphy, A. J., Myer, Y. P., and Vinogradov, S. N. (1965) Complex formation between methionine and a heme peptide from cytochrome *c*, *Proc. Natl. Acad. Sci. U.S.A. 54*, 1658−1664.
34. Kohler, M., Gafert, J., Friedrich, J., Vanderkooi, J. M., and Laberge, M. (1996) Stark effect experiments in cytochrome *c*-type proteins: Structural hierarchies, *Biophys. J. 71*, 77−85.
35. Fee, J. A., Chen, Y., Todaro, T. R., Bren, K. L., Patel, K. M., Hill, M. G., Gomez-Moran, E., Loehr, T. M., Ai, J., Thöny-Meyer, L., Williams, P. A., Stura, E., Sridhar, V., and McRee, D. E. (2000) Integrity of *Thermus thermophilus* cytochrome *c*(552) synthesized by *Escherichia coli* cells expressing the host-specific cytochrome *c* maturation genes, *ccmABCDEFGH*. Biochemical, spectral, and structural characterization of the recombinant protein, *Protein Sci. 9*, 2074−2084.
36. Timkovich, R., and Cai, M. L. (1993) Investigation of the structure of oxidized *Pseudomonas aeruginosa* cytochrome c_{551} by NMR—Comparison of observed paramagnetic shifts and calculated pseudocontact shifts, *Biochemistry 32*, 11516−11523.
37. Low, D. W., Gray, H. B., and Duus, J. Ø. (1997) Paramagnetic NMR spectroscopy of microperoxidase-8, *J. Am. Chem. Soc. 119*, 1−5.
38. Mondelli, R., Scaglioni, L., Mazzini, S., Bolis, G., and Ranghino, G. (2000) 3D structure of microperoxidase-11 by NMR and molecular dynamic studies, *Magn. Reson. Chem. 38*, 229−240.
39. Tachiiri, N., Hemmi, H., Takayama, S. J., Mita, H., Hasegawa, J., Sambongi, Y., and Yamamoto, Y. (2004) Effects of axial methionine coordination on the in-plane asymmetry of the heme electronic structure of cytochrome *c*, *J. Biol. Inorg. Chem. 9*, 733−742.
40. Banci, L., Bertini, I., Huber, J. G., Spyroulias, G. A., and Turano, P. (1999) Solution structure of reduced horse heart cytochrome *c*, *J. Biol. Inorg. Chem. 4*, 21−31.
41. Baistrocchi, P., Banci, L., Bertini, I., Turano, P., Bren, K. L., and Gray, H. B. (1996) Three-dimensional solution structure of *Saccharomyces cerevisiae* reduced iso-1-cytochrome *c*, *Biochemistry 35*, 13788−13696.
42. Chau, M.-H., Cai, M. L., and Timkovich. R. (1990) NMR comparison of prokaryotic and eukaryotic cytochromes *c*, *Biochemistry 29*, 5076−5087.
43. Tresoldi, G., Lo Schiavo, S., Lanza, S., and Cardiano, P. (2002) A congested Ru(dps)(2) or Ru(dprs)(2) core (dps = di-2-pyridyl sulfide; dprs = di-2-pyrimidinyl sulfide) promotes sulfur inversion of N,S-chelate thioethers containing CH2R and 2-pyridyl or 2-pyrimidinyl groups, *Eur. J. Inorg. Chem. 1*, 181−191.
44. Pollock, W. B. R., Rosell, F. I., Twitchett, M. B., Dumont, M. E., Mauk, A. G. (1998) Bacterial expression of a mitochondrial cytochrome *c*. Trimethylation of Lys72 in yeast iso-1-cytochrome *c* and the alkaline conformational transition, *Biochemistry 37*, 6124−6131.
45. Kellogg, J. A., and Bren, K. L. (2002) Characterization of recombinant horse cytochrome *c* synthesized with the assistance

of *Escherichia coli* cytochrome *c* maturation factors, *Biochim. Biophys. Acta 1601*, 215−221.
46. Berghuis, A. M., Guillemette, J. G., Smith, M., and Brayer, G. D. (1994) Mutation of tyrosine-67 to phenylalanine in cytochrome *c* significantly alters the local heme environment, *J. Mol. Biol. 235*, 1326−1341.
47. Lett, C. M., and Guillemette, J. G. (2002) Increasing the redox potential of isoform 1 of yeast cytochrome *c* through the modification of select haem interactions, *Biochem. J. 362*, 281−287.
48. Stuchebrukhov, A. A., and Marcus, R. A. (1995) Theoretical study of electron transfer in ferrocytochromes, *J. Phys. Chem. 99*, 7581−7590.
49. Detlefsen, D. J., Thanabal, V., Pecoraro, V. L., and Wagner, G. (1990) Sequential proton NMR assignments of iron(II) cytochrome-*c*551 from *Pseudomonas aeruginosa*, *Biochemistry 29*, 9377−9386.

BI047556+